

A sequential model for disaggregating near-surface soil moisture observations using multi-resolution thermal sensors

O. Merlin, A. Al Bitar, J P. Walker, Y.H. Kerr

► **To cite this version:**

O. Merlin, A. Al Bitar, J P. Walker, Y.H. Kerr. A sequential model for disaggregating near-surface soil moisture observations using multi-resolution thermal sensors. *Remote Sensing of Environment*, Elsevier, 2009, pp.RSE-07453; No of Pages 10. <10.1016/j.rse.2009.06.012>. <ird-00403130>

HAL Id: ird-00403130

<http://hal.ird.fr/ird-00403130>

Submitted on 9 Jul 2009

HAL is a multi-disciplinary open access archive for the deposit and dissemination of scientific research documents, whether they are published or not. The documents may come from teaching and research institutions in France or abroad, or from public or private research centers.

L'archive ouverte pluridisciplinaire **HAL**, est destinée au dépôt et à la diffusion de documents scientifiques de niveau recherche, publiés ou non, émanant des établissements d'enseignement et de recherche français ou étrangers, des laboratoires publics ou privés.



Contents lists available at ScienceDirect

Remote Sensing of Environment

journal homepage: www.elsevier.com/locate/rse

A sequential model for disaggregating near-surface soil moisture observations using multi-resolution thermal sensors

Olivier Merlin ^{a,*}, Ahmad Al Bitar ^a, Jeffrey P. Walker ^b, Yann Kerr ^a

^a Centre d'Etudes Spatiales de la Biosphère (CESBIO), Toulouse, France

^b Civil and Environmental Engineering, The University of Melbourne, Australia

ARTICLE INFO

Article history:

Received 9 April 2009

Received in revised form 16 June 2009

Accepted 20 June 2009

Available online xxx

Keywords:

Disaggregation

Soil moisture

Fractal

Scaling

Multi-sensor

NAFE

SMOS

MODIS

ASTER

ABSTRACT

A sequential model is developed to disaggregate microwave-derived soil moisture from 40 km to 4 km resolution using MODIS (Moderate Imaging Spectroradiometer) data and subsequently from 4 km to 500 m resolution using ASTER (Advanced Scanning Thermal Emission and Reflection Radiometer) data. The 1 km resolution airborne data collected during the three-week National Airborne Field Experiment 2006 (NAFE'06) are used to simulate the 40 km pixels, and a thermal-based disaggregation algorithm is applied using 1 km resolution MODIS and 100 m resolution ASTER data. The downscaled soil moisture data are subsequently evaluated using a combination of airborne and in situ soil moisture measurements. A key step in the procedure is to identify an optimal downscaling resolution in terms of disaggregation accuracy and sub-pixel soil moisture variability. Very consistent optimal downscaling resolutions are obtained for MODIS aboard Terra, MODIS aboard Aqua and ASTER, which are 4 to 5 times the thermal sensor resolution. The root mean square error between the 500 m resolution sequentially disaggregated and ground-measured soil moisture is 0.062 vol./vol. with a bias of -0.045 vol./vol. and values ranging from 0.08 to 0.40 vol./vol.

© 2009 Elsevier Inc. All rights reserved.

1. Introduction

Predicting the spatio-temporal variability of hydrological processes requires models that operate at different scales: evapotranspiration and infiltration at paddock-scale, run-off and drainage at catchment-scale, and atmospheric circulation at meso-scale. Due to the complexity of interacting processes (Chehbouni et al., 2008), the reliability of model predictions is intimately related to the ability to represent dominant processes in space and time using observations. Remote sensing has shown promise for this application due to its multi-resolution and multi-spectral capabilities (Choudhury, 1994).

Among the variables observable from space, soil moisture is one of the most crucial parameters that control hydrometeorological processes from paddock- to meso-scale. However, current and near-future spaceborne soil moisture products have a spatial resolution of several tens of kilometers (Crow et al., 2005) –about ~40 km resolution for the forthcoming Soil Moisture and Ocean Salinity (SMOS, Kerr et al., 2001) mission–, which make their application to hydrological and agricultural models challenging.

Downscaling methodologies are therefore needed to improve the spatial resolution of passive microwave-derived soil moisture. To understand how soil moisture scales, the spatial structure of soil moisture fields has been statistically described using experimental data sets aggregated at a range of resolutions. Those studies (e.g. Rodriguez-Iturbe et al., 1995; Das & Mohanty, 2008) conducted over different sites and using either remotely sensed or ground-based data, conclude that soil moisture behaves as a fractal –i.e. follows a power law decay– over a wide range of scales. Moreover, there is a general agreement that the fractal behaviour of soil moisture is not simple over extended scale ranges, and changes in time (Kim & Barros, 2002b; Dubayah et al., 1997; Western et al., 2002). In particular, the recent study of Das and Mohanty (2008) suggests a transition from simple fractal (in wet fields) to multi-fractal (in dry fields) behaviour during a dry-down period. In practice, the multi-fractal framework seems an appropriate basis for downscaling soil moisture fields in areas where ancillary data (e.g. topography, soil properties, vegetation, rainfall) are available at high resolution (Kim & Barros, 2002a).

One drawback with statistical approaches is that they require a large amount of data given that their validity domain is generally limited to the conditions used for calibration. Consequently, there is a need to develop methods that use physical and observable parameters. Bindlish and Barros (2002) developed an interpolation method to downscale L-band passive microwave data using active microwave data at the same wavelength to improve the resolution of

* Corresponding author.

E-mail address: olivier.merlin@cesbio.cnes.fr (O. Merlin).

brightness temperature fields prior to soil moisture retrieval. Similarly, Merlin et al. (2008a) developed a deterministic downscaling algorithm that combines 1 km resolution MODIS (MODerate resolution Imaging Spectroradiometer) data and a semi-empirical soil evaporative efficiency model. The main advantage of those approaches (Bindlish & Barros, 2002; Merlin et al., 2008a) over the purely empirical ones based on log–log plots (e.g. Kim & Barros, 2002a) is that some physical considerations are used to build a relationship between soil moisture and an ancillary observable; radar backscatter in Bindlish and Barros (2002) and soil evaporative efficiency in Merlin et al. (2008a).

In Merlin et al. (2008a), the disaggregation scale was fixed to 10 times the spatial resolution of MODIS thermal data to reduce the random uncertainties in disaggregated soil moisture. The authors observed that the sub-pixel variability of disaggregated soil moisture was significantly correlated with the observed fine-scale soil moisture variability, suggesting that the downscaling algorithm could be applied to spatial resolutions finer than 10 km. Nevertheless, that study did not apply the downscaling approach at multiple resolutions.

As a follow-up of Merlin et al. (2008a), this paper seeks to identify optimal downscaling resolutions in terms of disaggregation accuracy and sub-pixel spatial variability, and demonstrate the utility of this approach for sequential disaggregation of spaceborne surface soil moisture observations using multi-resolution thermal sensors. The development of a sequential approach is motivated by (i) the fact that high-resolution thermal data such as ASTER (Advanced Scanning Thermal Emission and Reflection Radiometer) data generally have a swath width smaller than the SMOS pixel and (ii) the hypothesis that the use of an intermediate resolution provides a better linearized approximation to a non linear function (e.g. soil evaporative efficiency model). One objective of the paper is to assess this hypothesis using data collected during the three-week National Airborne Field Experiment 2006 (NAFE'06). Airborne L-band data are used to simulate the 40 km resolution pixels expected from SMOS, and a thermal-based disaggregation algorithm is applied using MODIS and ASTER data. While the first part of the paper focuses on estimating optimal downscaling resolutions with MODIS and ASTER data, the second part takes advantage of these results to develop a sequential model for disaggregating ~40 km resolution microwave-derived soil moisture to 500 m.

2. Data

The NAFE'06 was conducted from 31 October to 20 November 2006 over a 40 km by 60 km area near Yanco (–35°N; 146°E) in southeastern Australia. While a full description of the data set is given in Merlin et al. (2008b), a brief overview of the most pertinent details are provided here. The data used in this study are comprised of wind speed measurements, L-band derived soil moisture and MODIS data collected over the Yanco area on twelve days, and ground measurements of 0–5 cm soil moisture and ASTER data collected over three 9 km² areas included in the Yanco area on one day (16 November) of the experiment.

2.1. Wind speed

Wind speed was monitored at 2 m by a meteorological station (located in the southwestern corner of the Yanco area, see Fig. 1 of Merlin et al. (2008b)) continuously during NAFE'06 with a time step of 20 min. The time series is illustrated in Fig. 1 of Merlin et al. (2008a).

2.2. Ground soil moisture

In situ measurements of 0–5 cm soil moisture were made using HDAS (Hydraprobe Data Acquisition System) on 16 November over

three 9 km² sampling areas (denoted as Y2, Y9 and Y12) included in the 40 km by 60 km Yanco area (Merlin et al., 2008b). Within each 9 km² sampling area, an average of three successive measurements was made ~1 m apart at each node of a 250 m resolution grid.

2.3. PLMR-derived soil moisture

The near-surface soil moisture was retrieved from the 1 km resolution brightness temperature collected by the Polarimetric L-band Multibeam Radiometer (PLMR) on eleven days over the 40 km by 60 km area: 31 October, 2, 3, 4, 5, 7, 9, 13, 14, 16, 18 November (Merlin et al., 2009). The surface temperature data used for the PLMR soil moisture inversion came from MODIS data on clear sky days, and from in situ measurements on overcast days. The root mean square difference between PLMR-derived and ground-measured soil moisture at 1 km resolution was estimated to 0.03 vol./vol. in non-irrigated areas. A bias of about –0.09 vol./vol. was obtained over pixels including some irrigation. This bias was explained by a difference in sensing depth between the L-band radiometer (~0–3 cm) and in situ measurements (0–5.7 cm), associated with a strong vertical gradient in the top 0–6 cm of the soil. Moreover on 3 November, which followed a rainfall event, the PLMR-derived soil moisture seemed to be affected by the presence of water intercepted by vegetation (Merlin et al., 2008b,a). In this study, data from this date were discarded.

2.4. MODIS data

The MODIS data used in this paper are the Version 5 MODIS/Terra (10:30 am) and MODIS/Aqua (1:30 pm) 1 km resolution daily surface temperature, and MODIS/Terra 250 m resolution 16-day Normalized Difference Vegetation Index (NDVI). The 16-day NDVI product was cloud free. In between the first (31 October) and last day (18 November) of 1 km resolution PLMR flights over the Yanco area, sixteen MODIS Version 5 surface temperature images with 0% cloud cover were acquired including nine aboard Terra (3, 5, 7, 8, 9, 10, 11, 17, 18 November) and seven aboard Aqua (31 October, 3, 4, 6, 8, 9, 17 November). Note that more cloud free images were obtained than from Version 4 surface temperature (Merlin et al., 2008a). The overestimation of cloud cover in Version 4 products and the subsequent increase of coverage in Version 5 land surface temperature products are discussed in Wan (2008). MODIS data were re-sampled on the same 1 km resolution grid as PLMR-derived soil moisture, and MODIS surface temperature was shifted of (+1 km E; –0.5 km N) and (+2 km E; 0 N) for Terra and Aqua respectively to maximize the spatial correlation with 1 km resolution MODIS NDVI, which was used as a reference for the co-registration.

2.5. ASTER data

The ASTER/Terra overpass of the NAFE'06 site was on 16 November 2006 at 10:30 am. Radiometric surface temperature was estimated from 90 m resolution L1B thermal radiances using the emissivity normalization method developed by Gillespie (1985) and Realmuto (1990) and implemented in ENVI (ENvironment for Visualizing Images, <http://www.itvis.com/envi/>) image processing software. Temperature was computed for each of the five thermal channels using a uniform emissivity set to 1, and the actual radiometric temperature was assumed to be equal to the highest computed temperature. Pre-processing of ASTER-derived radiometric temperature consisted of (i) registering the image with an accuracy better than 90 m from reference points (ii) extracting data over three 12 km by 12 km areas centered over the three 9 km² sampling areas, (iii) removing data that were visually identified as cloud or as cloud shade on the ground (note that the scene was cloud free over the three 9 km² sampling areas Y2, Y9 and Y12) and (iv) re-sampling data at 203 100 m resolution. An important point is that ASTER-derived radiometric surface temperature was not corrected for atmospheric effects. 205

The rationale is that only the spatial variability of surface temperature (about the mean) is used by the thermal-based disaggregation algorithm of Merlin et al. (2008a). In other words, there is no need for absolute values of surface temperature. Moreover, atmospheric corrections are generally made at a scale of several tens of kilometers (Thome et al., 1998), which is larger than the application scale (12 km in this study). Similar pre-processing was done on 15 m resolution ASTER red and near-infrared reflectances to derive 100 m resolution NDVI over the three 12 km by 12 km areas.

3. Towards an optimal downscaling resolution

The trade-off between downscaling resolution and accuracy within a disaggregation framework was already mentioned in a previous study (Merlin et al., 2008a). However, Merlin et al. (2008a) did not apply the downscaling approach at multiple resolutions. One objective of this paper is to identify the optimal downscaling resolution(s) in terms of disaggregation accuracy when using data from three sensors: MODIS aboard Terra, MODIS aboard Aqua and ASTER.

3.1. Approach

The approach adopted is to (i) aggregate reference (either PLMR-derived or HDAS-measured) soil moisture to the maximum spatial extent (40 km by 60 km for PLMR and 3 km by 3 km for HDAS), (ii) apply the disaggregation method at a range of resolutions, and (iii) compare the disaggregated soil moisture to the reference data for each downscaling resolution. The disaggregation of soil moisture thus requires simultaneous observations of surface temperature and NDVI. Moreover, validation requires soil moisture observations at a common spatial resolution. Among the twelve dates with at least one (either Terra or Aqua) MODIS image with 0% cloud cover, seven are concurrent with PLMR 1 km resolution flights. For the other five dates (6, 8, 10, 11 and 17 November), the PLMR-derived soil moisture data of the day before are used. This extrapolation is valid because no rainfall occurred between the PLMR flight and MODIS overpass on each date. Data are listed in Table 1.

Data derived from MODIS, PLMR, ASTER and HDAS are then aggregated to a range of spatial resolutions. MODIS surface temperature, MODIS NDVI and PLMR soil moisture are aggregated successively from 1 to 12 km in 1 km increments over the 40 km by 60 km area. Similarly, ASTER surface temperature, ASTER NDVI and HDAS soil moisture are aggregated successively from 100 to 1200 m in 100 m increments over the three 9 km² sampling areas. One should note that the spacing between ground measurements (250 m) was smaller than the two first aggregation resolutions (100 and 200 m). For these two resolutions, the pixels including no ground measurement were

discarded from the analysis and only pixels immediately over the ground measurement sites included. For simplicity, the different spatial resolutions will be denoted using the subscript n , varying from 1 (native resolution) to 12 (for instance, $SM_{PLMR,4}$ refers to PLMR-derived soil moisture aggregated at 4 km resolution and $SM_{mHDAS,5}$ refers to HDAS-measured soil moisture aggregated at 500 m resolution).

3.2. Disaggregation method

The thermal-based disaggregation approach used in this paper is that developed in Merlin et al. (2008a). The equations below represent the case of disaggregation using MODIS data for resolution pixels simulated by aggregating PLMR-derived soil moisture. Note that all equations also apply for disaggregation using ASTER data.

The soil moisture $SM_{MODIS,n}$ disaggregated at n km resolution at first order around the SMOS-resolution soil moisture $SM_{PLMR,40}$ is written as

$$SM_{MODIS,n} = SM_{PLMR,40} + \frac{\partial SM}{\partial SEE} \Delta SEE_{MODIS,n} \quad (1)$$

with $\partial SM/\partial SEE$ being the partial derivative (evaluated at $SM_{SMOS,40}$ of soil moisture to soil evaporative efficiency (SEE), and ΔSEE_n the difference between the MODIS-derived SEE estimated at n km resolution and its average within the SMOS pixel. Eq. (1) can be further simplified by using the simple expression of SEE from Komatsu (2003). The downscaling relationship becomes

$$SM_{MODIS,n} = SM_{PLMR,40} + SM_C \times SMP_{MODIS,n} \quad (2)$$

with SM_C being a semi-empirical parameter that depends on soil type and boundary layer conditions and SMP a normalized soil moisture proxy. In Merlin et al. (2008a), the SMP was defined as

$$SMP_{MODIS,n} = \frac{T_{MODIS,40} - T_{MODIS,n}}{T_{MODIS,40} - T_{min,1}} \quad (3)$$

with $T_{MODIS,n}$ being the soil temperature estimated using MODIS-derived NDVI and surface temperature, $T_{MODIS,40}$ its average within the SMOS pixel, and $T_{min,1}$ the minimum MODIS-derived soil temperature at 1 km resolution. Note that the minimum soil temperature was approximated to the minimum MODIS surface temperature. In Komatsu (2003), the parameter SM_C was calibrated for three different soils as function of wind speed

$$SM_C = SM_{C0} \left(1 + \frac{\gamma}{r_{ah}} \right) \quad (4)$$

with SM_{C0} (vol./vol.) being a soil-dependent parameter (ranging from about 0.01 vol./vol. for sand to 0.04 vol./vol. for clay), and r_{ah} (s m⁻¹) the aerodynamic resistance over bare soil. Aerodynamic resistance can be estimated from wind speed measurements u (m s⁻¹) at reference height Z (m) given the soil roughness z_{om} (m)

$$r_{ah} = \frac{1}{k^2 u} \left[\ln \left(\frac{Z}{z_{om}} \right) \right]^2 \quad (5)$$

with k being the von Karman constant. The soil temperature in Eq. (3) is estimated as

$$T_{MODIS,n} = \frac{T_{surf,MODIS,n} - f_{v,MODIS,n} T_{v,n}}{1 - f_{v,MODIS,n}} \quad (6)$$

with $T_{surf,MODIS,n}$ being the MODIS-derived surface temperature, $T_{v,n}$ the vegetation temperature, and $f_{v,MODIS,n}$ the fractional vegetation cover. In Merlin et al. (2008a), the vegetation temperature was approximated to

Table 1
List of acquisition dates, mean PLMR-derived soil moisture, wind speed measured at Terra (T) or Aqua (A) overpass time (10:30 am/1:30 pm), and minimum MODIS/Terra, MODIS/Aqua and ASTER surface temperature.

Date	$SM_{PLMR,40}$ vol./vol.	u (m s ⁻¹)		$T_{min,1}$ (°C)	ASTER
		T	A		
31 October	0.046		6.0		
4 November	0.11		7.6		
5 November	0.065	5.0		35.0	
6 November	0.065*		7.5		37.6
7 November	0.043	7.4		33.3	
8 November	0.043*	9.4	6.3	31.7	35.4
9 November	0.040	10.5	4.1	31.4	37.7
10 November	0.040*	11.9		36.1	
11 November	0.040*	5.3		36.8	
16 November	0.11	13.0			19.0
17 November	0.11*	4.5	3.6	32.2	36.3
18 November	0.055	5.1		34.7	

* PLMR data from the day before.

296 $T_{\min,1}$ by assuming that vegetation was not undergoing water stress, and
 297 fractional vegetation cover was estimated as

$$f_{v,MODIS,n} = \frac{NDVI_{MODIS,n} - NDVI_{\min}}{NDVI_{\max} - NDVI_{\min}} \quad (7)$$

298 with $NDVI_{\min}$ and $NDVI_{\max}$ being the NDVI value that corresponds to
 300 bare soil and fully vegetated pixels respectively.

301 In this study, parameters SM_{CO} , $NDVI_{\min}$ and $NDVI_{\max}$, as well as
 302 wind speed (r_{ah}) are assumed to be uniform within the SMOS pixel
 303 (model parameters are listed in Table 2). This invariance assumption
 304 will be further assessed in view of the disaggregation results obtained
 305 at a range of spatial resolutions.

306 3.3. Downscaling resolution versus disaggregation accuracy

307 Two different criteria are developed to estimate an optimal
 308 downscaling resolution for each of the three sensors. The first
 309 criterion denoted C1 is the condition that the disaggregation error
 310 evaluated at the downscaling resolution is equal to the observed sub-
 311 pixel variability. Intuitively, if the error on disaggregated soil moisture
 312 is smaller than the sub-pixel variability, then the downscaling
 313 resolution is too coarse to represent the actual variability; and
 314 conversely if the error is larger, then the downscaling resolution is
 315 too fine. C1 can be formulated as

$$RMSE_{n,n} = \overline{SD_{n,1}} \quad (8)$$

316 with $RMSE_{n,n}$ being the root mean square error evaluated at the
 318 (n km) disaggregation resolution between disaggregated and PLMR-
 319 derived soil moisture, and $\overline{SD_{n,1}}$ the mean standard deviation of 1 km
 320 resolution PLMR-derived soil moisture computed within each n^2 km²
 321 pixel. The n km resolution error is computed as

$$RMSE_{n,n} = \left[\frac{1}{N/n^2} \sum (SM_{MODIS,n} - SM_{PLMR,n})^2 \right]^{0.5} \quad (9)$$

322 with N being the number of 1 km resolution pixels within the 40 km
 324 by 60 km study area. The mean sub-pixel variability is computed as

$$\overline{SD_{n,1}} = \frac{1}{N/n^2} \sum SD_{n,1} \quad (10)$$

$$= \frac{1}{N/n^2} \sum \left[\frac{1}{n^2 - 1} \sum (SM_{PLMR,n} - SM_{PLMR,1})^2 \right]^{0.5} \quad (11)$$

328 The second criterion denoted C2 is the condition that the error
 329 evaluated at the native resolution ($n = 1$) is minimum. In other words,
 331 C2 is satisfied when the downscaling resolution makes the disag-
 332 gregation output the most accurate with respect to the reference soil
 333 moisture data obtained at the thermal sensor native resolution. C2 can
 334 be formulated as

$$RMSE_{n,1} = \left[\frac{1}{N} \sum (SM_{MODIS,n} - SM_{PLMR,1})^2 \right]^{0.5} \text{ is minimum} \quad (12)$$

336 with $RMSE_{n,1}$ being the root mean square error evaluated at 1 km
 337 resolution between the n km resolution disaggregated and 1 km
 338 resolution PLMR-derived soil moisture.

339 The criteria C1 and C2 can be applied to the three farms Y2, Y9 and
 340 Y12 by replacing in Eqs. (8) to (12), PLMR and MODIS by HDAS and
 341 ASTER respectively.

Table 2 Model parameters. t2.1

Parameter	Value	Unit	Source	t2.2
SM_{CO}	0.04	vol./vol.	Komatsu (2003)	t2.4
γ	100	s m ⁻¹	Komatsu (2003)	t2.6
Z_{0m}	0.005	m	Liu et al. (2007)	t2.7
$NDVI_{\min}$	0	–	Agam et al. (2007)	t2.8
$NDVI_{\max}$	1	–	Agam et al. (2007)	t2.8

342 3.4. Application to MODIS

The disaggregation algorithm of Eq. (2) is applied to each of the 343
 eight MODIS/Terra images (5, 7, 8, 9, 10, 11, 17 and 18 November) and 344
 to each of the six MODIS/Aqua images (31 October, 4, 6, 8, 9 and 17 345
 November), with a downscaling resolution ranging from 1 to 12 km. 346
 Fig. 1 plots the n km resolution disaggregated soil moisture versus the 347
 n km resolution PLMR-derived soil moisture for $n = 1, 2, 4, 8$ and 12. It 348
 is apparent that the noise on disaggregated soil moisture is 349
 successively reduced by increasing the downscaling resolution. 350
 However, the range of soil moisture values is also reduced and 351
 consequently the larger the resolution, the more limited the spatial 352
 representation of the actual soil moisture heterogeneity is. 353

As MODIS data were used for the PLMR soil moisture inversion, 354
 PLMR-derived and MODIS-disaggregated soil moisture are theoreti- 355
 cally not fully independent on clear sky days. However, it is argued 356
 that the cross-correlation of errors in the PLMR soil moisture 357
 measurements and the disaggregated soil moisture fields is not 358
 responsible for the good results in Fig. 1. One simple reason is that 359
 MODIS temperature has a positive impact on PLMR soil moisture 360
 retrievals (increasing with MODIS temperature) and a negative 361
 impact on disaggregated soil moisture (decreasing with MODIS 362
 temperature). Consequently, the cross-correlation of errors in PLMR- 363
 derived and MODIS-disaggregated soil moisture would actually make 364
 the results poorer. 365

Fig. 2 plots the $RMSE_{n,n}$ evaluated at the downscaling resolution as 366
 a function of n for each MODIS overpass date, separated according to 367
 Aqua and Terra data. The average for all dates is also plotted for each 368
 platform. The mean error decreases from about 0.045 vol./vol. at 1 km 369
 resolution to about 0.015 vol./vol. at 12 km resolution for both Aqua 370
 and Terra. On the same graph is plotted the mean sub-pixel variability 371
 $\overline{SD_{n,1}}$ for all dates. The mean sub-pixel variability increases from 0 to 372
 about 0.04 vol./vol. at 1 and 12 km resolution respectively for both 373
 Aqua and Terra. The standard deviation is equal to 0 at 1 km resolution 374
 because only one PLMR measurement is available per downscaled 375
 pixel at 1 km resolution. Following criterion C1 in Eq. (8), an optimal 376
 downscaling resolution exists where the RMSE and spatial variability 377
 lines cross. Inspection of Fig. 2 shows that the mean optimal resolution 378
 is about 3.7 km for MODIS aboard Aqua and 4.2 km for MODIS aboard 379
 Terra. Although relatively similar for both sensors, the RMSE of 380
 disaggregated soil moisture are remarkably more spread about the 381
 mean for Terra than for Aqua. The more consistent disaggregation 382
 results using MODIS/Aqua compared to MODIS/Terra was already 383
 mentioned in (Merlin et al., 2008a) when applied to 10 km resolution. 384
 This is due to the stronger coupling between SEE and soil moisture at 385
 1:30 pm than at 10:30 am. 386

Fig. 3 plots the average and standard deviation of the error $RMSE_{n,1}$ 387
 (evaluated at the thermal sensor native resolution) as a function n for 388
 Aqua and Terra data. The mean error is higher for Terra than for Aqua, 389
 which is consistent with previous results. For both Terra and Aqua, the 390
 mean error slightly decreases as spatial resolution increases from 1 to 391
 5 km, and slightly increases for spatial resolutions greater than 5 km. 392
 Following criterion C2, an optimal downscaling resolution is identified 393
 at about 5 km for both MODIS/Terra and MODIS/Aqua. Nevertheless, 394
 the minimum of $RMSE_{n,1}$ is not very well defined since the dynamics 395
 of the mean value are smaller than the variability observed within the 396

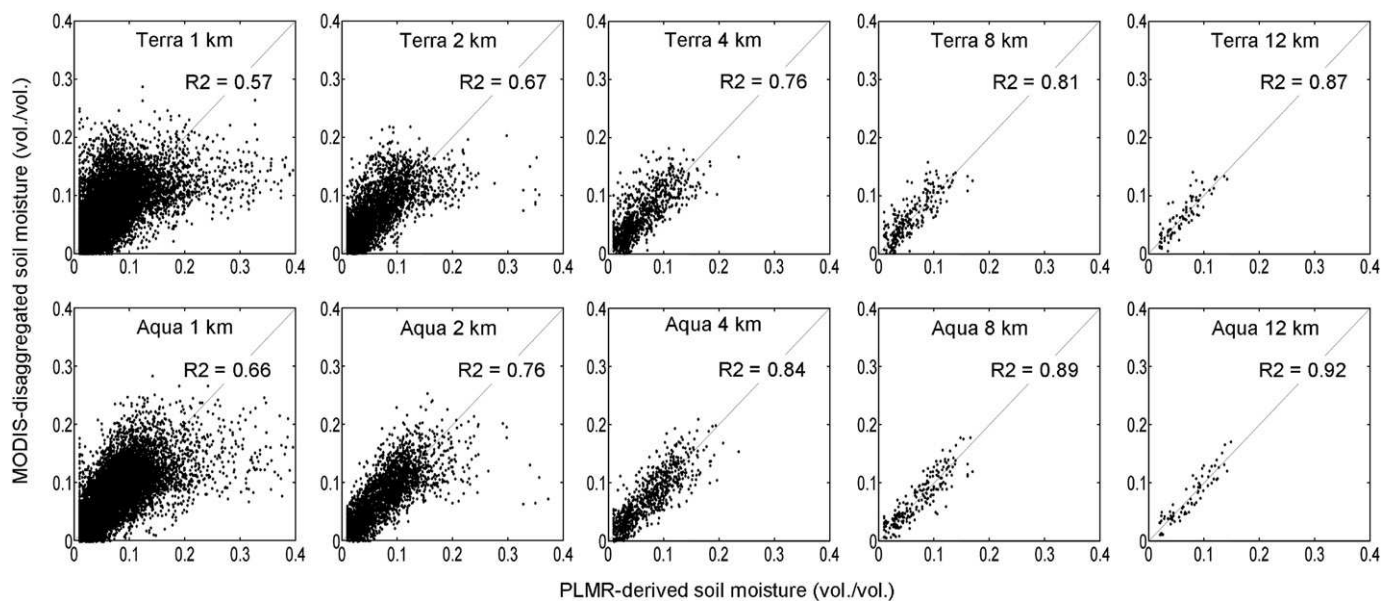


Fig. 1. Scatterplots of the MODIS-disaggregated versus PLMR-derived soil moisture using all twelve days of data for different downscaling resolutions: 1 km, 2 km, 4 km, 8 km and 12 km. The correlation coefficient R^2 is indicated on each plot.

397 data set (shown on Fig. 3 by the standard deviation σ). One limitation
 398 of the criterion C2 is that it includes both the uncertainty in the
 399 disaggregation output and the uncertainty in PLMR-derived soil
 400 moisture at the observation scale, so that the $RMSE_{n,1}$ can never be
 401 lower than the measurement error at the native resolution.

In summary, the application of criteria C1 and C2 to MODIS/PLMR
 data demonstrates that the optimal downscaling resolution in terms
 of disaggregation accuracy (using the NAFE'06 data set) is about 4 to
 5 km. Also, criterion C1 is better defined than C2 since it smooths out
 the uncertainties associated with random errors in PLMR-derived soil
 moisture.

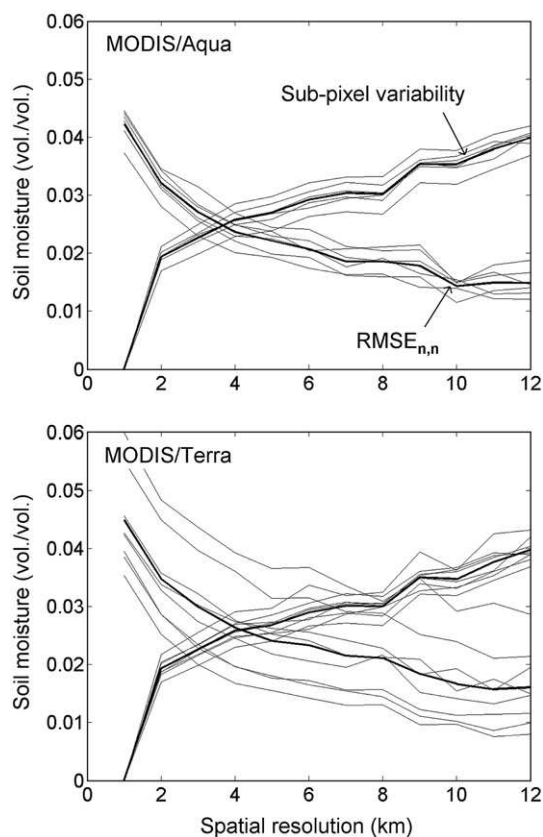


Fig. 2. Estimating an optimal downscaling resolution by comparing the root mean square error (RMSE) and the sub-pixel soil moisture variability at the disaggregation scale. The mean (thick line) RMSE is equal to the mean sub-pixel variability at about 4 km for both MODIS/Aqua and MODIS/Terra. The other lines represent the different dates.

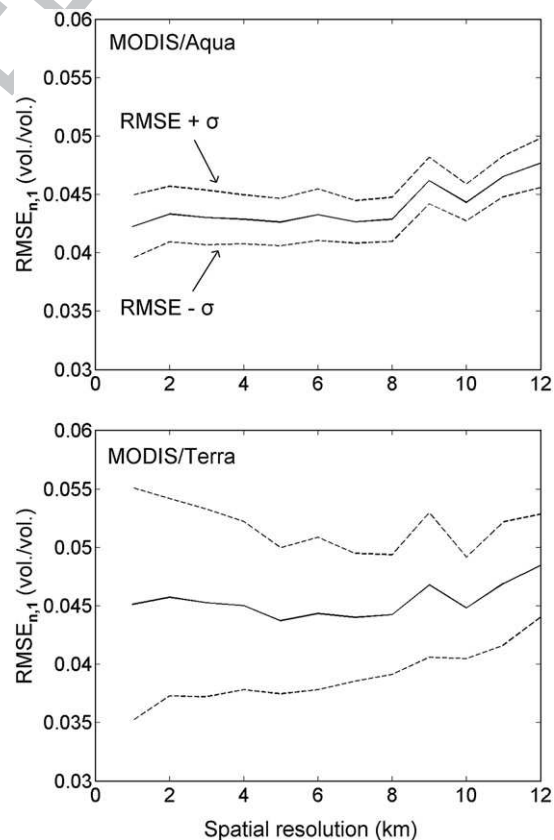


Fig. 3. Root mean square error (RMSE) evaluated at 1 km resolution for downscaling resolutions increasing from 1 to 12 km. Although the standard deviation (σ) between dates is high, the RMSE is minimum at 5 km for both MODIS aboard Aqua and MODIS aboard Terra.

3.5. Application to ASTER

The same disaggregation approach is applied to the three 9 km² sampling areas (Y2, Y9 and Y12) using the ASTER/HDAS data collected on 16 November, with a downscaling resolution ranging from 100 to 1200 m. Fig. 4 plots the $n \times 100$ m resolution disaggregated soil moisture versus the $n \times 100$ m resolution aggregated HDAS measurements for $n = 1, 2, 4, 5, 8$ and 12. As with MODIS/PLMR data, it is apparent that the accuracy on disaggregated soil moisture increases (and the range of downscaled values decreases) as the downscaling resolution increases. In Fig. 4, three data points are clearly aside from the 1:1 line for downscaling resolutions of 100 m and 200 m. These correspond to the pixels that included a portion of rice field in Y9. Since rice crops were flooded during NAFE'06, no HDAS measurement was made. Consequently, the nearby ground measurements did not represent well the overall “wetness” (including both soil moisture and standing water) of the surface that the disaggregation algorithm actually represents.

When comparing Figs. 1 and 4, one observes that the disaggregation approach is much more accurate when applied to MODIS data than when applied to ASTER data. In particular for $n = 8$, the correlation coefficient is about 0.80 for MODIS and 0.60 for ASTER. The relatively poor results obtained using ASTER data can be interpreted as a consequence of the spatial variability of soil moisture at fine scale. As the typical crop size in the study area was about 100–300 m, soil moisture fields were much more heterogeneous at 100 m resolution than at 1 km and above. It is suggested that point-scale measurements aggregated at 100–1000 m resolution were generally more uncertain than 1 km resolution remotely-sensed PLMR-derived soil moisture.

Fig. 5 plots the $RMSE_{n,n}$ evaluated at the downscaling resolution as a function of n . It is apparent that the error is approximately constant at 100 m and 200 m resolution, which is consistent with the fact that the spacing (250 m) of HDAS measurements was larger than the thermal sensor native resolution so that the spatial variability of HDAS measurements is not represented below 300 m. For all farms, the error is maximum at 200 m, and is minimum at 1200 m resolution with a value of about 0.02 vol./vol. On the same graph is plotted the mean sub-pixel variability $SD_{n,1}$ for each farm. The mean variability is about 0.02 vol./vol. at $n = 1$ and is generally maximum at $n = 12$. Note that

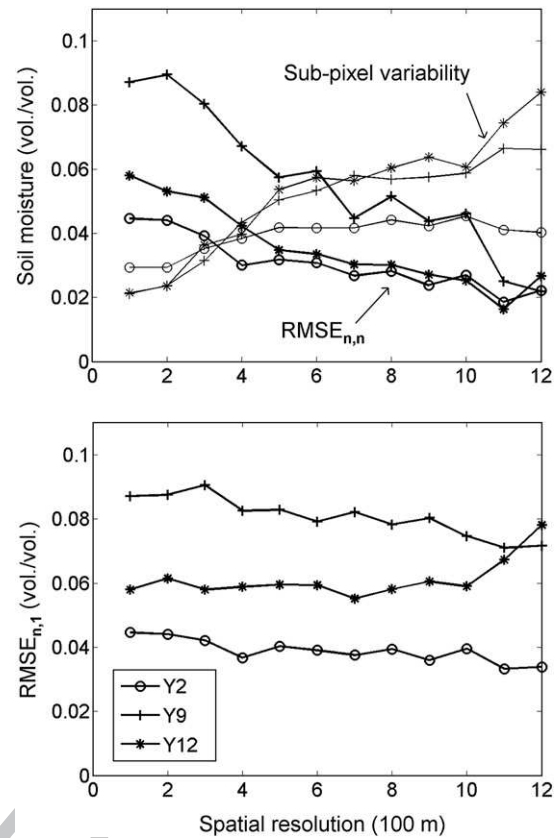


Fig. 5. Root mean square error (RMSE) evaluated at the downscaling resolution (top) and at 100 m resolution (bottom) for downscaling resolutions increasing from 100 to 1200 m.

its value at $n = 1$ is not equal to zero as in the case of PLMR data, 447 because three successive measurements were made at each sampling 448 point, providing the mean local-scale variability of HDAS measure- 449 ments. Following criterion C1 in Eq. (8), the optimal downscaling 450 resolution for each farm is identified at 300 m, 400 m and 600 m for 451 Y2, Y9 and Y12 respectively. 452

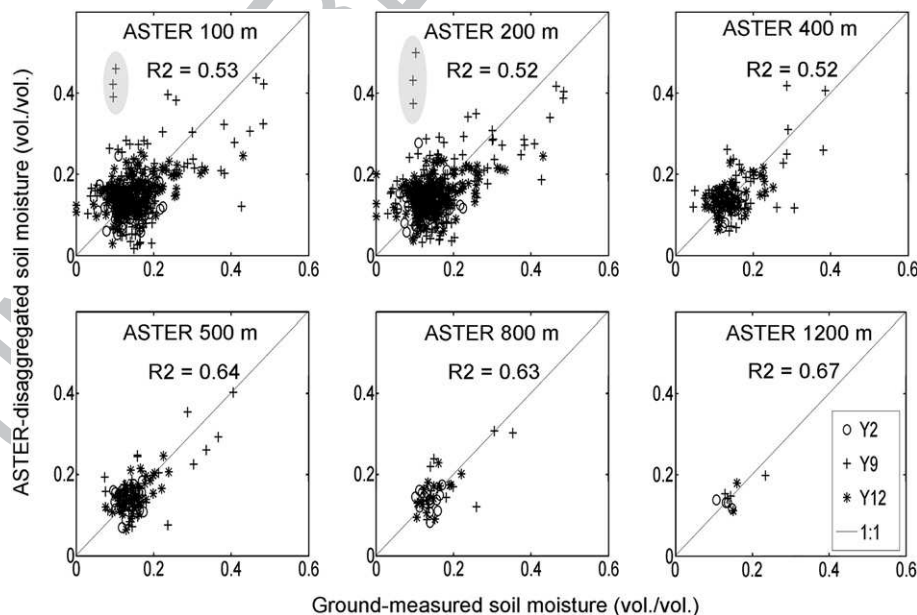


Fig. 4. Scatterplots of the ASTER-disaggregated versus ground-measured soil moisture on 16 November for different downscaling resolutions: 100 m, 200 m, 400 m, 500 m, 800 m and 1200 m. Highlighted pluses correspond to pixels containing standing water (flooded rice fields). The correlation coefficient R2 is indicated on each plot.

453 Fig. 5 also plots the error $RMSE_{n,1}$ evaluated at the ASTER native
 454 resolution (100 m) as a function of n . Although one observes a minimum
 455 of the error for Y12 at $n = 7$, no minimum is observed for the other farms
 456 (Y2 and Y9). Several hypotheses can be postulated to explain these
 457 contrasting results. First, when using ground measurements instead of
 458 airborne L-band data, reference soil moisture data are representative of
 459 the point-scale and may not be representative of the scales integrated to
 460 several hundreds of meters, especially over highly heterogeneous
 461 irrigated areas like in Y9. Second, the farm-scale variability in Y2 was
 462 about the same as the local-scale variability (uncertainty in a single
 463 HDAS measurement). Consequently, the disaggregation over that farm
 464 was not expected to improve the accuracy of soil moisture at fine scale.
 465 Third, it was seen in the case of MODIS/PLMR that criterion C2 was not
 466 very stable from date to date, so no clear result can be expected from
 467 only one date with ASTER/HDAS.

468 In summary, the application of criteria C1 and C2 to ASTER/HDAS
 469 data suggests that the optimal downscaling resolution in terms of
 470 disaggregation accuracy (using the NAFE'06 data set) is about 4 to 5
 471 times the thermal sensor resolution. Criterion C1 is again found to be
 472 better defined than C2.

473 4. Sequential disaggregation

474 The general approach of the sequential disaggregation using multi-
 475 resolution thermal sensors is presented in Fig. 6. The ~40 km resolution
 476 SMOS-scale soil moisture generated from PLMR data on 16 November is

disaggregated at an intermediate resolution (4 km in Fig. 6) using
 477 MODIS data and the MODIS-disaggregated soil moisture is disaggre-
 478 gated again at a finer resolution using ASTER data. Note that the MODIS
 479 data on 16 November were not cloud free over the 40 km SMOS-scale
 480 pixel so that the MODIS data on 17 November were used instead. 481

482 4.1. A sequential model

The sequential model is written as 483

$$SM_{S_{i+1}} = SM_{S_i} + \frac{\partial SM}{\partial SEE} \Delta SEE_{S_{i+1}} \quad (13)$$

with S_i being the sensor of index i . In our case, S_0 , S_1 and S_2 484
 corresponds to SMOS, MODIS and ASTER respectively. By using this 486
 notation, Eqs. (2) and (3) become 487

$$SM_{S_{i+1}} = SM_{S_i} + SM_C \times SMP_{S_{i+1}} \quad (14)$$

with 488

$$SMP_{S_{i+1}} = \frac{T_{S_i} - T_{S_{i+1}}}{T_{S_i} - T_{min}} \quad (15)$$

From the above equations, one is able to identify the parameters that 490
 do not vary with scale. In particular, the minimum soil temperature 492

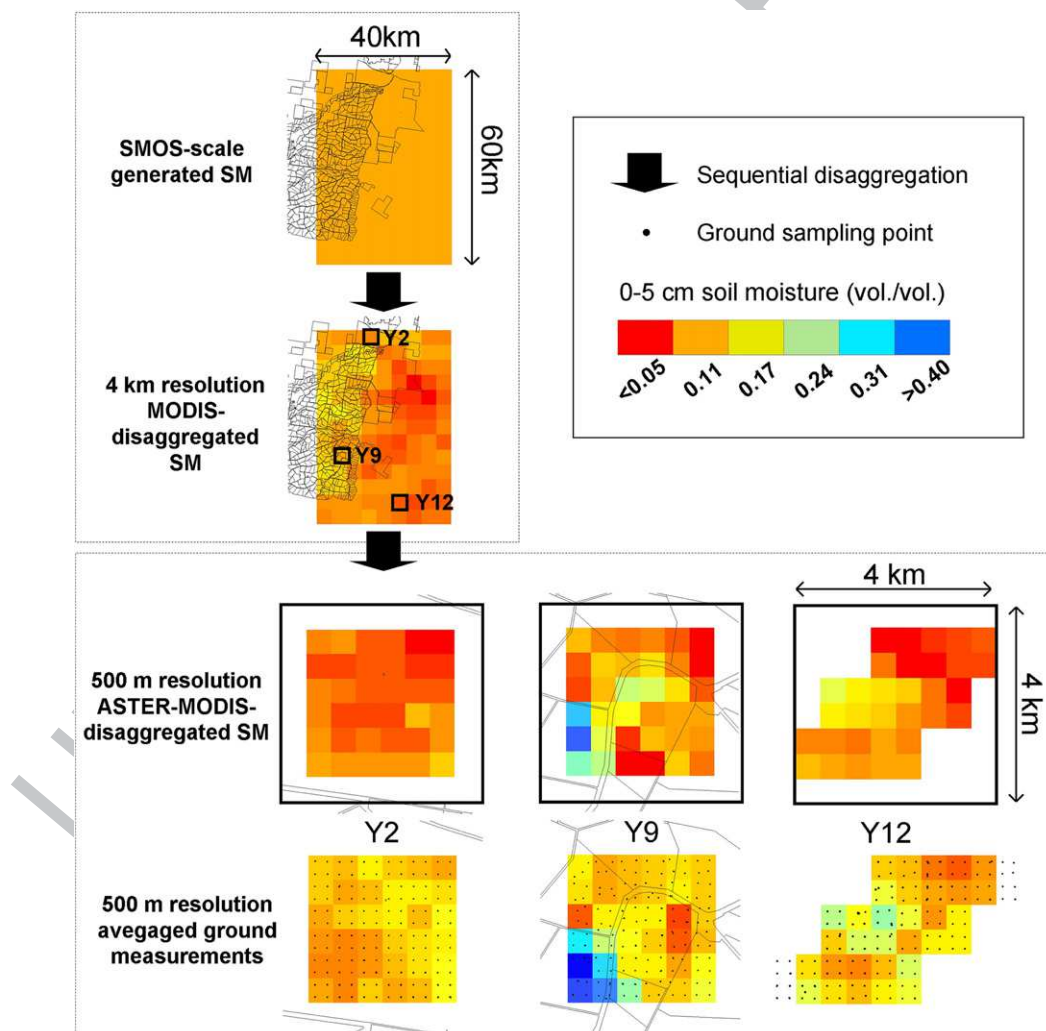


Fig. 6. Schematic diagram presenting the sequential disaggregation of SMOS-scale soil moisture using MODIS and ASTER data.

493 T_{\min} and the soil property SM_C are assumed to be scale-invariant. An
 494 important point is that these assumptions might not be valid in the
 495 case of heterogeneous soil within the SMOS-scale pixel. In particular,
 496 Merlin et al. (2008a) demonstrated that estimating SM_C at high
 497 resolution improved significantly the disaggregation accuracy. How-
 498 ever, the scale-invariance of SM_C was not tested in this paper since
 499 only one ASTER image was available whereas a time series would be
 500 required (Merlin et al., 2008a).

501 4.2. Application

502 Based on the results of the previous section, the intermediate
 503 resolution is set to four times the MODIS native resolution (4 km) and
 504 the target resolution to five times the ASTER native resolution
 505 (500 m). In practice, three data sets were derived by defining a
 506 4 km resolution pixel centered on each of the three sampling areas
 507 (see black outlines in Fig. 6). This pixel was used to create over the
 508 SMOS-scale pixel a 4 km resolution grid, on which the 1 km resolution
 509 MODIS and PLMR data were aggregated. The sequential model of
 510 Eq. (14) was finally applied to each data set.

511 Fig. 7 plots the 4 km resolution MODIS-disaggregated soil moisture
 512 versus the 4 km resolution PLMR-derived soil moisture for each of the
 513 three data sets. The root mean square error is 0.026 vol./vol. Fig. 7 also
 514 plots the 500 m resolution ASTER-MODIS-disaggregated soil moisture
 515 versus the 500 m resolution HDAS-measured soil moisture in each
 516 farm. The sequentially disaggregated soil moisture has a RMSE of
 517 0.062 vol./vol. and a bias of -0.045 vol./vol. Results are degraded
 518 compared to the case when the ASTER-disaggregated soil moisture
 519 was based on HDAS-aggregated measurements and not on MODIS-
 520 disaggregated soil moisture. The increase of uncertainty could be due

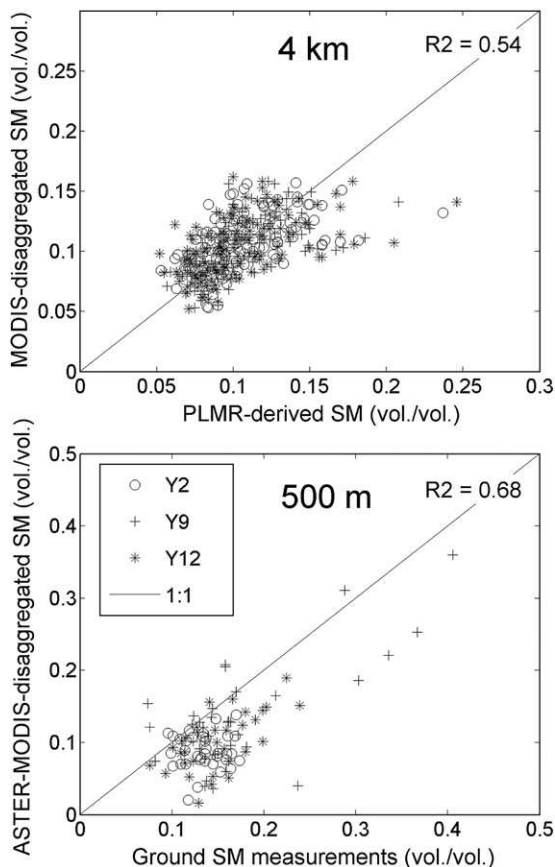


Fig. 7. Scatterplots of the 4 km resolution MODIS-disaggregated versus 4 km aggregated PLMR-derived soil moisture (top) and the 500 m resolution ASTER-MODIS-disaggregated versus 500 m HDAS measurements (bottom).

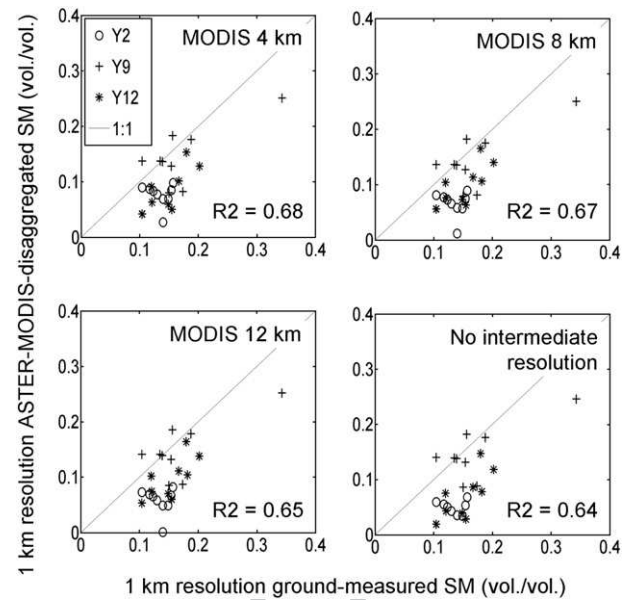


Fig. 8. Scatterplots of the 1 km resolution ASTER-MODIS-disaggregated soil moisture versus HDAS measurements for three different intermediate resolutions: 4 km, 8 km and 12 km, and for the case of "no intermediate resolution".

to the disaggregation method and/or the soil moisture retrieval
 521 algorithm. The bias on disaggregated soil moisture is estimated as
 522 -0.047 , -0.040 and -0.049 vol./vol. for Y2, Y9 and Y12 respectively.
 523 Although a persistent bias of about -0.045 vol./vol. tends to
 524 corroborate the hypothesis of a bias in the PLMR-derived soil moisture
 525 on 16 November, no conclusion can be drawn from only three
 526 independent data sets.

Errors on disaggregated soil moisture might also come from the
 528 disaggregation method itself, which may not fully represent the non-
 529 linear behaviour of the relationship between SEE and soil moisture.
 530 The effect of this non-linearity is clearly visible in Fig 7 where MODIS-
 531 disaggregated soil moisture tends to saturate at PLMR-derived soil
 532 moisture values higher than 0.20 vol./vol. Moreover, our sequential
 533 model did not account for the propagation of errors in the
 534 disaggregation. In particular, a random error in MODIS-disaggregated
 535 soil moisture at 4 km resolution would behave as a bias on 500 m
 536 resolution ASTER-MODIS-disaggregated soil moisture within each
 537 4 km resolution pixel.

One way to limit the increase of uncertainty associated with error
 539 propagations would be to choose a coarser target resolution. In
 540

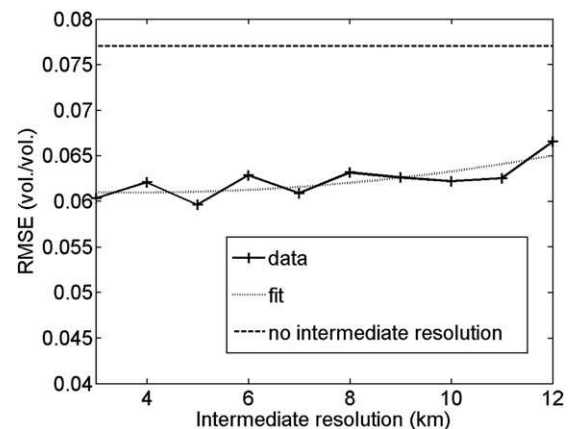


Fig. 9. Root mean square error on the 1 km resolution ASTER-MODIS-disaggregated soil moisture for an intermediate resolution increasing from 3 to 12 km. The error obtained in the case of "no intermediate resolution" is also indicated.

particular, output errors are expected to be reduced by setting the downscaling resolution to a value larger than the resolution that was found to be optimal when using one sensor (MODIS or ASTER) independently from the combination of both.

4.3. Sensitivity to intermediate resolution

Due to propagation errors from the coarser to finer resolutions, the combination of multi-source (MODIS and ASTER) data is likely to increase the disaggregation uncertainty. Consequently, one may argue that a more efficient approach than combining MODIS and ASTER data would be the direct disaggregation of SMOS-scale soil moisture using ASTER data only. The point is the swath width of ASTER (60 km) is much narrower than that of SMOS (~1000 km). In particular, the 40 km by 60 km area covered by PLMR (SMOS-scale pixel) during NAFE'06 was not entirely covered by ASTER. Therefore, the disaggregation of SMOS-scale soil moisture requires thermal data at an intermediate resolution (MODIS) before the use of high-resolution (ASTER) data over smaller focus areas.

To assess the sensitivity of disaggregation results to intermediate resolution, an additional analysis is presented. The target resolution is now fixed to 1 km, and the intermediate resolution is increased from 3 to 12 km in 1 km increments. The 1 km resolution ASTER-MODIS-disaggregated soil moisture is then compared to ground measurements aggregated at 1 km resolution. Pre-processing included (i) defining a pixel with a resolution ranging from 3 to 12 km and covering each of the three 9 km² sampling areas (ii) creating a 3–12 km resolution grid over the SMOS-scale pixel based on that pre-defined pixel and (iii) aggregating 1 km resolution MODIS and PLMR data at 3–12 km resolution on that pre-defined grid. The sequential model of Eq. (14) was finally applied to each data set for an intermediate resolution ranging from 3 to 12 km.

Fig. 8 plots the 1 km resolution ASTER-MODIS-disaggregated versus HDAS-measured soil moisture for three different intermediate resolutions: 4, 8 and 12 km and for the case of “no intermediate resolution”. For the case “no intermediate resolution”, the SMOS pixel is disaggregated at 1 km resolution directly using only the ASTER data. As the ASTER image did not entirely cover the SMOS pixel, the mean temperature required in Eq. (15) was estimated within the overlap area of ASTER and PLMR data, which represented about 80% of the SMOS pixel. The RMSE on sequentially disaggregated soil moisture is 0.060 and 0.077 vol./vol., the bias -0.049 and -0.063 vol./vol., and the correlation coefficient 0.68 and 0.64 at 4 km and 12 km resolution respectively. The error is plotted as a function of intermediate resolution in Fig. 9. It is apparent that the error is minimum at 3–5 km and slightly increases with intermediate resolution, meaning that the optimal intermediate resolution is the highest. Note that the oscillation of the RMSE around its upward trend is mainly due to the change of the spatial extent of input data each time data are aggregated to a different intermediate resolution. For intermediate resolutions ranging from 3 to 12 km, the error is lower than that obtained in the case of “no intermediate resolution”. This shows that the use of MODIS data in the sequential disaggregation increases the accuracy on ASTER-disaggregated soil moisture. It is suggested that the use of an intermediate resolution between SMOS and ASTER is able to reduce the non-linearity effects across scales between soil evaporative efficiency and soil moisture, despite the increase of uncertainties associated with error propagations.

5. Conclusion

A sequential model was developed to disaggregate microwave-derived soil moisture recursively from 40 km to 4 km resolution using MODIS data and from 4 km to 500 m resolution using ASTER data. The airborne and ground data collected during the three-week NAFE'06 were used to simulate coarse-scale pixels, and a thermal-based

disaggregation algorithm was applied using 1 km resolution MODIS and 100 m resolution ASTER data. A key step in the procedure was to identify an optimal downscaling resolution in terms of disaggregation accuracy and sub-pixel soil moisture variability by using two criteria. The first criterion C1 was to look for the spatial resolution such that the RMSE evaluated at the downscaling resolution be equal to the sub-pixel soil moisture variability, while the second criterion C2 was to look for the spatial resolution that minimized the RMSE evaluated at the thermal sensor native resolution (1 km for MODIS or 100 m for ASTER). Very consistent optimal downscaling resolutions were obtained for MODIS aboard Terra, MODIS aboard Aqua and ASTER, which were 4 to 5 times the thermal sensor resolution.

The 40 km resolution SMOS-scale soil moisture generated from airborne L-band data on 16 November was disaggregated at an intermediate resolution (4 km) using MODIS data and the MODIS-disaggregated soil moisture was disaggregated again at 500 m resolution using ASTER data. The RMSE between the 500 m resolution sequentially-disaggregated and ground-measured soil moisture was 0.062 vol./vol. with a bias of -0.045 vol./vol. and soil moisture values ranging from 0.08 to 0.40 vol./vol. To assess the impact of the intermediate resolution on disaggregation accuracy, a different approach was proposed by setting the target resolution to 1 km and by increasing the intermediate resolution from 3 to 12 km. The optimal intermediate resolution was found to be 3–5 km, meaning that the use of MODIS data reduced the non-linearity effects across scales between SMOS and ASTER resolutions, despite the increase of uncertainties associated with the combination of MODIS and ASTER data.

Beyond the application of multi-resolution soil moisture data to a range of environmental sciences, such an approach could greatly facilitate the validation of coarse-scale microwave-derived soil moisture data using point-scale ground measurements. The sequential model is being implemented over the Valencia Anchor Station area (Lopez-Baeza et al., 2007) in the SMOS calibration/validation framework.

Note that the operational application of thermal-based methods would require high-spatial-resolution thermal data acquired at high-temporal-resolution, typically 2–3 days. However, high-spatial-resolution (ASTER-like) thermal data are currently available on a monthly basis, which raises the issue of disaggregating low-spatial-resolution (MODIS-like) thermal data at high-temporal-resolution (Agam et al., 2007).

Refinements of the sequential disaggregation method would include a physical calibration of the soil evaporative efficiency model, which is at present semi-empirical. Moreover, the disaggregation accuracy is affected by the non-linearity of that exponential function. Recent developments have accounted for the non-linearity of the models used in the disaggregation of remote sensing data with the projection technique (Merlin et al., 2006) or the Taylor series including derivative terms at orders superior to 1. The applicability of those approaches and their stability still need to be confirmed at a range of spatial resolutions.

Acknowledgements

The NAFE'06 participants are gratefully acknowledged for their participation in collecting this extensive data set. The National Airborne Field Experiments have been made possible through infrastructure (LE0453434 and LE0560930) and research (DP0557543) funding from the Australian Research Council, and the collaboration of a large number of scientists from throughout Australia, United States and Europe. Initial setup and maintenance of the study catchments was funded by a research grant (DP0343778) from the Australian Research Council and by the CRC for Catchment Hydrology. This work was funded by the French program Terre-Océan-Surface-Atmosphère and the Centre National de la Recherche Scientifique.

References

- 667
668 Agam, N., Kustas, W. P., Anderson, M. C., Li, F., & Neale, C. M. U. (2007). A vegetation
669 index based technique for spatial sharpening of thermal imagery. *Remote Sensing of*
670 *Environment*, 107, 545–558.
- 671 Bindlish, R., & Barros, A. P. (2002). Subpixel variability of remotely sensed soil moisture:
672 An inter-comparison study of SAR and ESTAR. *IEEE Transactions on Geoscience and*
673 *Remote Sensing*, 40, 326–337.
- 674 Chehbouni, A., Escadafal, R., Duchemin, B., Boulet, G., Simonneaux, V., Dedieu, G.,
675 Mougenot, B., Khabba, S., Kharrou, H., Maisongrande, P., Merlin, O., Chaponnière, A.,
676 Ezzahar, J., Er-Raki, S., Hoedjes, J., Hadria, R., Abourida, A., Cheggour, A., Raibi, F.,
677 Boudhar, A., Benhadj, I., Hanich, L., Benkaddour, A., Guemouria, N., Chehbouni, A. H.,
678 Lahrouni, A., Olioso, A., Jacob, F., Williams, D. G., & Sobrino, J. A. (2008). An integrated
679 modelling and remote sensing approach for hydrological study in arid and semi-arid
680 regions: The SUDMED Programme. *International Journal of Remote Sensing*, 29(17),
681 5161–5181.
- 682 Choudhury, B. J. (1994). Synergism of multispectral satellite observations for estimating
683 regional land surface evaporation. *Remote Sensing of Environment*, 49(3), 264–274.
- 684 Crow, W. T., Ryu, D., & Famiglietti, J. S. (2005). Upscaling of field-scale soil moisture
685 measurements using distributed land surface modeling. *Advances in Water*
686 *Resources*, 28(1), 1–14.
- 687 Das, N. N., & Mohanty, B. P. (2008). Temporal dynamics of PSR-based soil moisture
688 across spatial scales in an agricultural landscape during SMEX02: A wavelet
689 approach. *Remote Sensing of Environment*, 112, 522–534.
- 690 Dubayah, R., Wood, E. F., & Lvallee, D. (1997). Multiscaling analysis in distributed modeling
691 and remote sensing: An application using soil moisture. In D. A. Quattrochi, & M.
692 Goodchild (Eds.), *Scale in Remote Sensing and GIS* New York: Lewis Publisher.
- 693 Gillespie, A. R. (1985). Lithologic mapping of silicate rocks using TIMS. *The TIMS Data*
694 *User's Workshop* (pp. 29–44). Pasadena, CA: JPL pub Vol. 86–38.
- 695 Kerr, Y. H., Waldteufel, P., Wigneron, J.-P., Martinuzzi, J.-M., Font, J., & Berger, M. (2001).
696 Soil moisture retrieval from space: The soil moisture and ocean salinity (SMOS)
697 mission. *IEEE Transactions on Geoscience and Remote Sensing*, 39, 1729–1735.
- 698 Kim, G., & Barros, A. P. (2002). Downscaling of remotely sensed soil moisture with a
699 modified fractal interpolation method using contraction mapping and ancillary
700 data. *Remote Sensing of Environment*, 83, 400–413.
- 701 Kim, G., & Barros, A. P. (2002). Space-time characterization of soil moisture from passive
702 microwave remotely sensed imagery and ancillary data. *Remote Sensing of*
703 *Environment*, 81, 393–403.
- Komatsu, T. S. (2003). Towards a robust phenomenological expression of evaporation
704 efficiency for unsaturated soil surfaces. *Journal of Applied Meteorology*, 42, 1330–1334. 705
- Liu, S., Mao, D., & Jia, L. (2007). Evaluating parameterizations of aerodynamic resistance
706 to heat transfer using field measurements. *Hydrology and Earth System Science*, 11, 707
769–783. 708
- Lopez-Baeza, E., Vidal, S., Cano, A., Domenech, C., Geraldo-Ferreira, A., Millan-Scheiding, 709
C., Narbon, C., Sanchis, J., & Velazquez, A. (2007). Representativity of the Valencia 710
and the Alacant anchor stations in the context of validation of remote sensing 711
algorithms and low-resolution products. *Proceedings of the Joint 2007 EUMETSAT 712*
Meteorological Satellite Conference and the 15th Satellite Meteorology and Oceanog-
raphy Conference of the American Meteorological Society. Amsterdam. 713
714
- Merlin, O., Chehbouni, G., Kerr, Y., & Goodrich, D. (2006). A downscaling method for 715
distributing surface soil moisture within a microwave pixel: Application to the 716
Monsoon'90 data. *Remote Sensing of Environment*, 101, 379–389. 717
- Merlin, O., Walker, J. P., Chehbouni, A., & Kerr, Y. (2008). Towards deterministic 718
downscaling of SMOS soil moisture using MODIS derived soil evaporative efficiency. 719
Remote Sensing of Environment, 112, 3935–3946. doi:10.1016/j.rse.2008.06.012. 720
- Merlin, O., Walker, J. P., Kalma, J. D., Kim, E. J., Hacker, J., Panciera, R., Young, R., 721
Summerell, G., Hornbuckle, J., Hafeez, M., & Jackson, T. J. (2008). The NAFE'06 data 722
set: Towards soil moisture retrieval at intermediate resolution. *Advances in Water 723*
Resources, 31, 1444–1455. doi:10.1016/j.advwatres.2008.01.018. 724
- Merlin, O., Walker, J. P., Panciera, R., Escorihuela, M. J., & Jackson, T. J. (2009). Assessing 725
the SMOS soil moisture retrieval parameters with high-resolution NAFE'06 data. 726
Geoscience Remote Sensing Letters. doi:10.1109/LGRS.2008.2012727. 727
- Realmutto, V. J. (1990). Separating the effects of temperature and emissivity: Emissivity 728
spectrum normalization. *2nd TIMS Workshop* (pp. 310–316). Pasadena, CA: JPL pub 729
Vol. 90–55. 730
- Rodriguez-Iturbe, I., Vogel, G. K., & Rigon, R. (1995). On the spatial organization of soil 731
moisture fields. *Geophysical Research Letters*, 22(20), 2757–2760. 732
- Thome, K., Palluconi, F., Takashima, T., & Masuda, K. (1998). Atmospheric correction of 733
ASTER. *IEEE Transactions on Geoscience and Remote Sensing*, 36(4), 1199–1211. 734
doi:10.1109/36.701026. 735
- Wan, Z. (2008). New refinements and validation of the MODIS land-surface temperature/
736 emissivity products. *Remote Sensing of Environment*, 112(1), 59–74. doi:10.1016/j.
737 rse.2006.06.026. 738
- Western, A. W., Grayson, R. B., & Blöschl, G. (2002). Scaling of soil moisture. *Annual 739*
Review Earth Planetary Science, 30, 149–180. 740

Q2